



## Research article

# Prediction of textural properties of 3D-printed food using response surface methodology

Cheng Pau Lee<sup>a,b</sup>, Michinao Hashimoto<sup>a,b,\*</sup><sup>a</sup> Pillar of Engineering Product Development, Singapore University of Technology and Design, 8 Somapah Road Singapore, 487372, Singapore<sup>b</sup> SUTD-MIT International Design Centre (IDC), Singapore University of Technology and Design, 8 Somapah Road Singapore, 487372, Singapore

## ARTICLE INFO

## Keywords:

3D food printing  
Response surface methodology  
Food texture  
Insect protein

## ABSTRACT

3D printing has enabled modifying internal structures of the food affecting textural properties, but predicting desired texture remains challenging. To overcome this challenge, the use of response surface methodology (RSM) was demonstrated to develop empirical models relating 3D printing parameters to textural properties using aqueous inks containing cricket powders as a model system. Regression models were established for our key textural properties (*i.e.*, hardness (*H*), adhesiveness (*A*), cohesiveness (*C*), and springiness (*S*)) in response to three 3D printing parameters: infill percentage (*i*), layer height (*h*), and print speed (*s*). Our developed model successfully predicted the 3D printing parameters to achieve the intended textural properties using a multi-objective optimization framework. The predicted limits for *H*, *A*, *C*, and *S* were 0.66–5.39 N, 0.01–12.43 mJ, 0.01–1.05, and 0–19.20 mm, respectively. To validate our models, we simulated the texture of other food using our model ink and achieved high accuracy for *H* (99%), *C* (82%), and *S* (87%). This work highlights a simple way to 3D-print foods with spatially different textures and materials, unlocking the full potential of 3D printing technology for manufacturing a range of customized foods.

## 1. Introduction

This paper describes a method to predict and control the texture of 3D-printed food using response surface methodology (RSM). Recent advances in 3D printing have enabled automated 3D fabrication of foods with different internal structures that offer unique textures for consumption [1–3]. However, because of the large number of variables involved in 3D printing, predicting and achieving the desired textural properties of 3D-printed foods from a single food material remains challenging. Existing methods have employed the one-factor-at-a-time (OFAT) approach, which involves varying one variable at a time while holding the other variables constant. In this work, statistical analysis was applied to derive empirical models relating essential 3D printing parameters to the textural properties of 3D-printed models using three key input parameters: (1) infill percentage (*i*), (2) layer height (*h*), and (3) print speed (*s*). The empirical model allowed predicting four textural properties of the 3D-printed foods: hardness (*H*), adhesiveness (*A*), cohesiveness (*C*), and springiness (*S*) using a model ink consisting of cricket powders and hydrocolloids. Extending the demonstration, we fabricated a single 3D-printed model harboring spatially distinct infill percentages within the structure to demonstrate the potential of the developed method to produce food with unique textures. Overall, this work has enabled prediction and achieving desired texture for

\* Corresponding author. Pillar of Engineering Product Development, Singapore University of Technology and Design, 8 Somapah Road Singapore, 487372, Singapore.

E-mail address: [hashimoto@sutd.edu.sg](mailto:hashimoto@sutd.edu.sg) (M. Hashimoto).

<https://doi.org/10.1016/j.heliyon.2024.e27658>

Received 28 February 2024; Accepted 5 March 2024

Available online 6 March 2024

2405-8440/© 2024 Published by Elsevier Ltd.

This is an open access article under the CC BY-NC-ND license

(<http://creativecommons.org/licenses/by-nc-nd/4.0/>).

3D-printed foods through the use of RSM.

3D printing is a method of digital fabrication where materials are patterned to create a 3D object using a computer-designed model. The technology is employed across multiple materials and applications to realize cell-laden constructs [4–6], metal parts [7–9], microfluidic devices [10–13], and electronic devices [14,15]. Food printing is one of the emerging applications of the technology. Direct ink writing (DIW) is one of the established methods for food printing capable of patterning a broad range of edible materials such as chocolate [16–18], milk [19,20], hydrogels [21,22], and vegetables [23–25]. 3D food printing offers benefits in the customization of nutrients based on individual requirements [26,27], fabrication of aesthetically pleasing meals [28,29], and modification of internal structures of the food [3]. The modification of internal structures has demonstrated the control of food texture of the food, which allows creating unique textures for consumption [2,30].

The modification of food texture is conducted to meet different consumer preferences and acceptance levels. For example, food must be made soft to masticate, and smooth to swallow, for dysphagic patients who have difficulty in initiation of swallowing [31]. In this study, food textures refer to the physical attributes including hardness, adhesiveness, and gumminess. These textural properties can be evaluated through objective measurements such as texture profile analysis (TPA). Previous works have shown that 3D printing parameters have major influences on textural properties such as hardness. It was reported that the infill percentage of 3D-printed chocolate influenced the hardness of the product—an increase in infill percentage increases the hardness of the chocolate, suggesting that the textural properties can be controlled by the internal configuration of the printed food [2,30]. Another study reported that features of the mouthfeel experience such as perceived ease of bite and number of cracks could be controlled by tailoring the fracture properties of 3D-printed chocolate [32]. Despite the ability to modify food textural properties by 3D printing, studies often performed one-factor-at-a-time (OFAT) experiments; OFAT experiments vary only one variable at a time while keeping other variables constant. For example, a study investigated the effect of internal structure on the texture of air-fried yam snacks by varying (1) different ink formulations, (2) infill percentages, and (3) infill patterns, each factor at a time [33]. As 3D printing involves multiple variables for operation of the instrument and printing materials, considering only one variable at a time may fail to account for the effects of multiple variables and their interdependence.

Functioning as a mathematical and statistical technique in experimental design, RSM has proven instrumental in optimizing the effects of process variables [34]. RSM has been extensively applied in the optimization of mechanical properties in 3D-printed objects [35,36]. Studies have successfully enhanced tensile and puncture strength in edible films by strategically designing ink formulations [37]. In 3D food printing, the use of RSM allowed the formulation of inks for 3D-printed chicken products and the intricate construction of egg white protein objects [38,39]. Yet another study investigated the impact of process parameters, such as infill and patterns, on the chewing time of 3D-printed food [40]. While these research works have significantly advanced the field, there is a lack of a systematic approach to predict and control textural properties that account for multiple printing variables simultaneously.

To bridge this gap, this work aimed to create a method to develop an empirical model that accounts for multiple 3D printing parameters to predict the texture of 3D-printed food. We employed RSM to generate a model for textural properties. The central composite design (CCD) (*i.e.*, an experimental design in RSM) was applied to fit second-order response surface models for the textural responses. Using a model food ink consisting of 40% w/w cricket powder with 0.4% w/w xanthan gum, the structures were fabricated according to the design of experiments and texture profile analyses were performed. We tested the accuracy of our models by simulating the texture of other food using our model ink and the accuracy of the developed models for hardness, adhesiveness, cohesiveness, and springiness were 99%, 50%, 82%, and 87% respectively. Overall, these results affirmed the validity of our approach to control the texture of food. Extending the demonstration, we printed cricket steaks with multiple domains with different infill percentages to demonstrate food with varying textures. The principles and methods discussed in this work should apply to other edible inks to achieve desired textural properties or replicate the texture of other foods.

## 2. Materials and methods

### 2.1. Preparation of cricket ink

Acheta Domesticus cricket powder (Thailand Unique, Thailand) and xanthan gum (Better4U, Singapore) were commercially available. The cricket powder was sifted with a 300- $\mu\text{m}$  sieve (Industrial and Laboratory Consumables, China) to obtain powders with a powder size of less than 300  $\mu\text{m}$ . The thickener was prepared using 0.4% w/w xanthan gum and water. The cricket ink was formulated by mixing 40% w/w cricket powder and the thickener with a planetary centrifugal mixer (Thinky ARE-250, Thinky Corporation, Tokyo, Japan) for 5 min at 2000 revolutions per minute (rpm) at room temperature ( $\sim 25^\circ\text{C}$ ). The inks were left to sit for at least 30 min before 3D printing.

### 2.2. Rheological characterization

Rheological properties of the food ink were measured with an oscillatory rheometer (Discovery Hybrid Rheometer DHR-2, TA Instruments, Delaware, USA). Stainless steel parallel plates with a diameter of 25 mm and a truncation height of 1000  $\mu\text{m}$  were used for all measurements. Viscosity tests were conducted by applying a stepwise shear rate ramp for 0.01–100  $\text{s}^{-1}$ . Stress sweep measurements were conducted with a logarithmically increasing shear stress at a constant frequency of 1 Hz over 0.1–4000 Pa to determine the viscoelastic properties of the samples. Flow ramp tests were conducted at four stages with varying shear rates: (1) 0.1–1  $\text{s}^{-1}$  for 60 s, (2) 0.1–200  $\text{s}^{-1}$  for 2 s, (3) 200–0.1  $\text{s}^{-1}$  for 2 s, and (4) 0.1–1  $\text{s}^{-1}$  for 60 s. An excess material outside the parallel plates was removed before each measurement to prevent the edge effect. All rheological measurements were conducted at room temperature on triplicates.

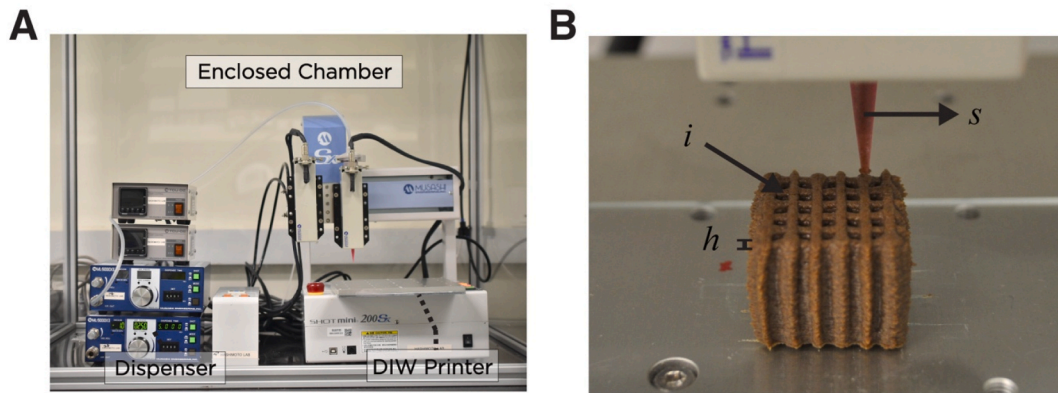


**Fig. 1.** Photographs of the setup for direct ink writing (DIW) 3D printing of cricket ink at room temperature. **A)** DIW system used in the experiment. **B)** Controllable factors (3D printing parameters) used in the experiment (1) infill percentage ( $i$ ), (2) layer height ( $h$ ), and (3) print speed ( $s$ ).

### 2.3. DIW 3D printing

3D printing was done using a pneumatic extrusion-based DIW printer (SHOTmini 200 Sx, Musashi Engineering, Inc., Tokyo, Japan) (Fig. 1). The speed and printing path were controlled through MuCAD V software (Musashi Engineering, Inc., Tokyo, Japan) developed for this printer. A 3D model was designed on Solidworks (Dassault Systèmes, Waltham, MA, USA), a computer-aided design (CAD) software. The designed 3D model was then converted to stereolithography (STL) file format in Solidworks. Slic3r, an open-source software was used to generate the G-code. The infill level was adjusted in Slic3r. The generated G-code was converted to MuCAD V code via a programming script written in Python and loaded to the DIW printer. All samples were loaded into a 50-mL Luer lock dispensing syringe (V-S liquid control equipment, China) fitted with a 20 G nozzle (Birmingham Gauge) (V-S liquid control equipment, China). All substrates used in this work were glass slides (Matsunami Glass Ind., Ltd, Osaka, Japan). Before printing, the standoff distance between the substrate and nozzle was calibrated to the layer thickness using a height feeler gauge (QST Express-01, China). The dispensing pressure was kept constant at 0.200 MPa. All printings were conducted at room temperature in a chamber to maintain a sterile environment.

### 2.4. Response surface modelling

The input variables examined in this work were infill percentage ( $i$ ), layer height ( $h$ ), and print speed ( $s$ ). The infill was created as a mesh consisting of straight lines and printed in a rectilinear pattern. The infill percentage represents the volume of the interior space within the designed model, calculated based on a fixed width of 0.6 mm (nozzle diameter) and the spacing between the lines designed for printing; the layer height is the thickness of each deposited layer; the print speed is the speed of the print head during the printing. Four textural properties—(1) hardness ( $H$ ), (2) adhesiveness ( $A$ ), (3) cohesiveness ( $C$ ), and (4) springiness ( $S$ )—were studied [41]. To determine the effect of the print parameters and the interaction among them on the textural properties, RSM experimental design was carried out to reduce the required number of experiments [34]. A CCD at five levels of each factor, with an  $\alpha$ -value of  $\pm 1.682$ , was applied (Fig. S1). A total of 34 measurements (consisting of eight replicates of factorial points, three replicates of center points, and six replicates of axial) were performed and characterized for the response of each textural property. The CCD was ensured to be rotatable, where the axial points are located at a distance of  $\alpha$  from the center, such that the variance of the predicted responses was the same for all  $x_i$  and  $x_j$ . The  $\alpha$  is defined by:

$$\alpha = (F)^{\frac{1}{4}}$$

where  $F$  is the number of factorial points ( $2^k$ ). Our CCD consisted of  $2^3$  factorial points, six center points, and six axial points with an axial spacing ( $\alpha$ ) of 1.682. The regression analyses were performed on all responses to construct a second-order polynomial. All statistical analyses were performed using statistical software (Minitab, Pennsylvania, USA).

### 2.5. Texture profile analysis (TPA)

The texture profile analysis was conducted on the 3D-printed cricket samples using a 10-kg load texture analyzer (CT3 Texture Analyzer, Brookfield, USA). The samples were of a fixed size, measuring 15 mm in length, width, and height. The texture analyzer was first calibrated with a 10-kg weight before any measurements were conducted. The printed cricket samples were fixed at the center of the fixture base table before the measurements. All texture profile analysis measurements were conducted with a cylindrical probe with a diameter of 38.1 mm, at a pre-test speed of 2.0 mm/s, test speed of 2.0 mm/s, post-test speed of 2.0 mm/s, trigger load of 5.0 g, and compression strain of 45% to determine the four textural properties ( $H$ ,  $A$ ,  $C$ , and  $S$ ). Since the CCD is specifically designed to balance the trade-off between experimental efficiency and result precision, the replicates included in our design were statistically

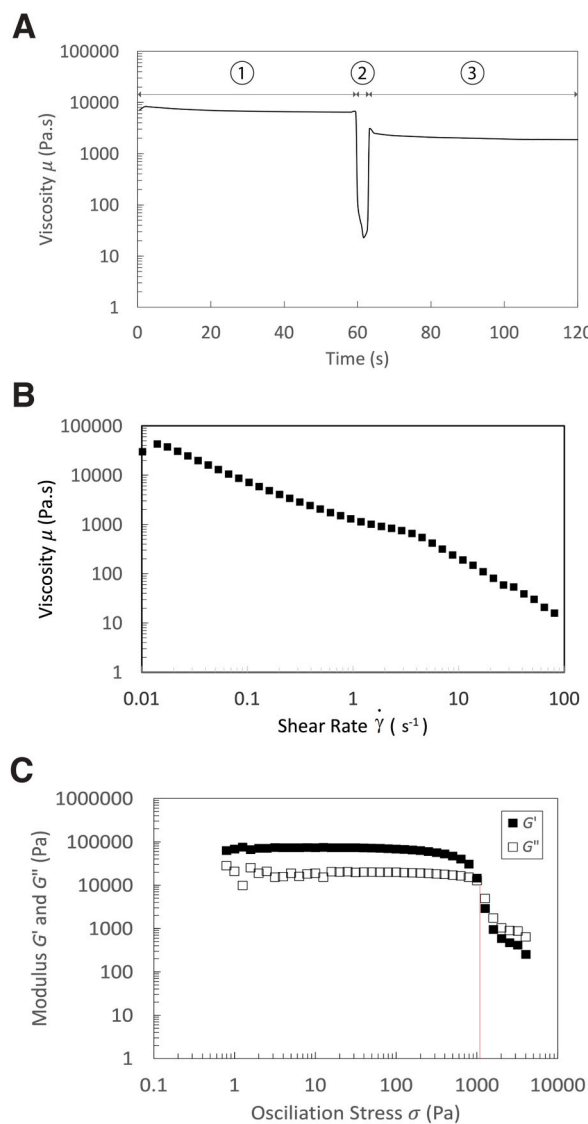


**Fig. 2.** Rheological characterization of cricket ink. **A**) Representative viscosity of cricket ink ( $\mu$ ) with changing shear rate ( $\dot{\gamma}$ ) over time: (1) before extrusion, (2) during extrusion, and (3) after extrusion through the nozzle. **B**) Viscosity ( $\mu$ ) as a function of applied shear rate ( $\dot{\gamma}$ ). **C**) Storage moduli ( $G'$ ) and loss moduli ( $G''$ ) as a function of applied oscillatory shear stress ( $\sigma$ ). Yield stress corresponds to the crossover point between storage and loss modulus.

justified to capture variability and provide meaningful insights into the effects being studied. Therefore, all TPA measurements were conducted at room temperature on duplicate samples. To validate the accuracy of the model, the texture profile of locally sourced mashed potatoes was analyzed and compared against the texture profile of 3D-printed cricket samples.

### 3. Results and discussion

#### 3.1. Selection of food ink

In this work, the cricket ink was selected as a model food ink for 3D printing. There is growing interest in using insects as alternative food sources [42]. Insects are generally considered safe for human consumption and are a good source of protein, vitamins, essential fatty acids, and crude fiber [42]. Crickets serve as an immense source of protein containing up to 78% of protein, 6.7% of fats, 5.5% of carbohydrate, and 5.4% of crude fibers [43]. Moreover, it also contains a substantial amount of vitamins and minerals such as vitamin B12, calcium, potassium, and iron [43]. However, the consumption of insects is not well received by people due to its poor aesthetics despite the nutritious value of insects. 3D printing may serve as a potential route to alter the appearance of such foods. When insects are

utilized as food ink for 3D printing, they are used as a form of powders (*i.e.*, microparticles). The high-protein powder is difficult to suspend in water due to its propensity to coagulate and form clumps, which could potentially cause nozzle clogging and therefore hinder the 3D printing process. Nevertheless, the use of insect powders in 3D printing holds immense potential, as they are sustainable and eco-friendly sources of protein. 3D printing with insect proteins can lead to the development of novel food textures and appearances that could enhance the overall appeal of insects as food sources, ultimately increasing their acceptability among consumers [44]. This study hence aimed to use RSM to control the textural properties of cricket inks, allowing for potential applications such as replicating the texture of other foods by adjusting the printing parameters or blending cricket inks with other food inks to create unique mouthfeel sensations.

### 3.2. Formulation of the ink

To prepare an extrudable food ink, sifting was performed to reduce the particle size to  $<300\ \mu\text{m}$ . Inks consisting of controlled particle sizes are crucial to achieving reproducible rheological properties [1]. Particles larger than  $300\ \mu\text{m}$  were not used in the experiments. In the first iteration of our experimentation, the cricket ink formulation was tested without any hydrocolloid, resulting in nozzle clogging. Subsequently, similarly to previous works [24,45,46], xanthan gum was used to modify the rheological properties of the food ink. Previous research demonstrated successful formulation of printable ink using 0.3–1% xanthan gum. Therefore, a fixed amount of xanthan gum was incorporated within this range. Our final ink formulation comprised 40% w/w cricket ink with 0.4% w/w xanthan gum), which was observed to be effectively deposited without broken lines (Fig. S2).

### 3.3. Rheological characterization of cricket ink

Ink recovery experiments were conducted to simulate the three stages of extrusion printing: before extrusion, during extrusion, and after extrusion through the nozzle. The cricket ink was able to restore its viscosity after the removal of yield stress (Fig. 2A). This observation suggested that the structure of the printed ink was maintained after extrusion. The formulated cricket ink displayed shear thinning behavior; the viscosity decreased from  $\sim 10^3$  to  $\sim 10^1$  Pa·s with an increasing shear rate between  $0.01\ \text{s}^{-1}$  and  $100\ \text{s}^{-1}$  (Fig. 2B). Oscillation amplitude tests were performed to determine the storage modulus ( $G'$ ) and loss modulus ( $G''$ ); these parameters allow understanding of the viscoelastic property of the ink matrix. A linear viscoelastic region (LVR) was observed where  $G'$  was  $67000 \pm 300$  Pa which ensured the structural integrity of the printed material after deposition (Fig. 2C). High values of  $G'$  suggested the physicochemical interactions within the inks are strong, and such inks would offer robust structures. Both  $G'$  and  $G''$  started to deviate from linearity due to the deformation of the bonds within the ink, suggesting the yielding of the ink at  $1050 \pm 50$  Pa that led to liquid-like behavior (Table S1). In a previous study, inks with a yield stress of 106 Pa and a storage modulus of 19 kPa were found to be adequately printed using a DIW printer [19]. The yield stress and storage modulus were higher than these reported values, indicating that it possessed the necessary rheological properties for printability.

### 3.4. Selection of process parameters

3D food printing involves a series of processes that affect the texture of printed products. These processes occur in three stages: 1) extrusion, 2) printing, and 3) post-processing. Firstly, factors such as nozzle diameter, applied pressure, and the rheological properties of inks affect the extrusion of inks. Extrusion-based DIW printers employ diverse systems, including piston, pneumatic, or screw-based mechanisms. Each system operates with different extrusion parameters, such as motor speed or pneumatic pressure, which directly control the rate of extrusion. The parameters under extrusion determine the mass flow rate of the materials extruded from the given nozzle.

Secondly, the 3D printing process involves parameters that can be controlled through the robotic system. The CAD design of the object decides the overall shape of the 3D object, and the toolpath is determined based on the CAD design with multiple parameters. Parameters such as infill percentage, layer height, and print speed determine the locally deposited amount of the ink. For example, the infill percentage determines the density of the internal structure. The layer height determines the thickness of each printed layer, and the print speed inversely affects the amount of materials extruded per unit length. A past study has shown that the print speed has a significant influence on the width of printed structures [47]. In this research work, we study the influence of these printing parameters on the textural properties while maintaining the extrusion parameters constant. For the consistent extrusion of the food ink, a specific nozzle size (20 G, approximately  $603\ \mu\text{m}$  in ID) was chosen to prevent material blockage and ensure seamless extrusion. This choice took into account the diameter of the particles (less than  $300\ \mu\text{m}$ ) to avoid clogging of the nozzle.

Lastly, post-processing treatments can modify the composition or structure of the printed products, thereby affecting their textural properties. Variables include temperature, humidity, and duration of the treatment. These treatments occur after the printing process is completed and do not directly control how the material is deposited and structured during printing. While post-processing certainly affects the textural properties, the focus of the current study lies primarily on understanding the direct influence of the 3D printing process on the textural properties. To ensure consistency and reproducibility, we standardized our extrusion process by selecting key controllable parameters that directly affect the printing outcomes. Overall, this research aimed to study the influence of the variables pertaining to the printing by the robotic control (*i.e.*, infill percentage ( $i$ ), layer height ( $h$ ), and print speed ( $s$ )) on the textural properties in this study.

	<i>i</i>	<i>h</i>	<i>s</i>	Run 1	Replicate
FACTORIAL	-1	-1	-1		
	1	-1	-1		
	-1	1	-1		
	1	1	-1		
	-1	-1	1		
	1	-1	1		
	-1	1	1		
AXIAL	-1.682	0	0		
	1.682	0	0		
	0	-1.682	0		
	0	1.682	0		
	0	0	-1.682		
	0	0	1.682		
CENTER	0	0	0		
	0	0	0		
	0	0	0		

**Fig. 3.** Design of experiments, and the printed models of cricket inks with eight factorial points, six axial points ( $\alpha$ -value =  $\pm 1.682$ ), and three center points. Experiments were conducted in duplicates. (Scale bar: 5 mm).

**Table 1**

Analysis of variance (ANOVA) for hardness.

Source	Degree of freedom	Adjusted sum of squares	Adjusted mean square	F-Value	P-Value
Model	10	37.1517	3.7152	98.12	<0.001
<i>i</i>	1	31.124	31.124	822.04	<0.001
<i>h</i>	1	4.1073	4.1073	108.48	<0.001
<i>s</i>	1	0.4305	0.4305	11.37	0.003
<i>i</i> <sup>2</sup>	1	0.3227	0.3227	8.52	0.008
<i>h</i> <sup>2</sup>	1	0.0956	0.0956	2.52	0.126
<i>s</i> <sup>2</sup>	1	0.0287	0.0287	0.76	0.393
<i>i</i> <sup>2</sup> <i>h</i>	1	0.6162	0.6162	16.28	0.001
<i>i</i> <sup>2</sup> <i>s</i>	1	0.1089	0.1089	2.88	0.103
<i>h</i> <sup>2</sup> <i>s</i>	1	0.164	0.164	4.33	0.049
Error	23	0.8708	0.0379		
Lack-of-Fit	19	0.7877	0.0415	1.99	0.265
Pure Error	4	0.0831	0.0208		
Total	33	38.0225			

### 3.5. Response surface modelling (RSM)

The structures were printed based on the design of experiments (Fig. 3) and the textural responses were measured (Table S3). The analysis of variance (ANOVA) was conducted for each textural response to generate a polynomial model that relates to the 3D printing parameters (Table 1). The model for hardness is a good fit, as evidenced by its *P*-value of <0.001. Moreover, the *P*-value of lack-of-fit is >0.05 (*P* = 0.265), indicating that the lack of fit for the model is not significant. Table 1 illustrates that the *P*-value for *i*, *h*, *s*, *i*<sup>2</sup>, (*i*)(*h*) and (*h*)(*s*) were <0.05, which indicates that they are significant and should be considered in the model. The *P*-value for *h*<sup>2</sup> and (*i*)(*s*), are >0.05, and these terms were excluded from the model. Similar approaches were performed for the other three textural responses:

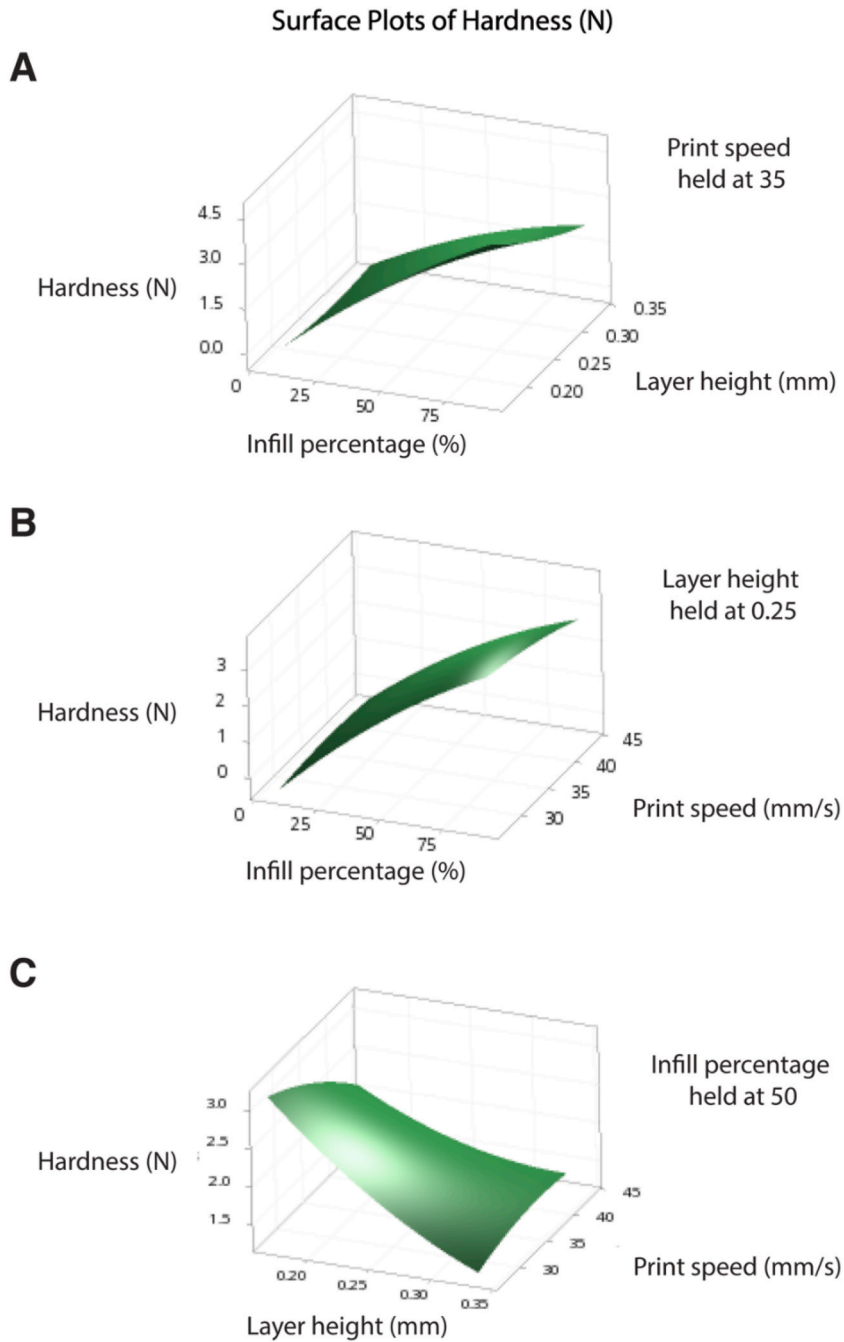


**Fig. 4.** Response surface plots for hardness: **A)** Hardness as a function of infill percentage (%) and layer height (mm) **B)** Hardness as a function of infill percentage (%) and print speed (mm/s) **C)** Hardness as a function of layer height (mm) and print speed (mm/s). Note that other textural properties (adhesiveness, cohesiveness, and springiness) are summarized in Supplementary Information (Figs. S3, S4, and S5).

adhesiveness (*A*), cohesiveness (*C*), and springiness (*S*). The surface models for all textural responses were calculated as follows:

$$H = 2.42 + 0.1242i - 27.1h + 0.006s - 0.000191i^2 - 0.1570ih + 0.405hs \tag{1}$$

$$A = -0.8 + 0.310i + 52.7h - 0.598s \tag{2}$$

$$C = 0.87 + 0.00816i + 8.66h - 0.1007s + 0.002142s^2 \tag{3}$$

**Table 2**  
Predicted limits of responses with corresponding parameters.

Response	Range		Min. level settings			Max. level settings		
	Min	Max	<i>i</i> (%)	<i>h</i> (mm)	<i>s</i> (mm/s)	<i>i</i> (%)	<i>h</i> (mm)	<i>s</i> (mm/s)
Hardness (N)	0.66	5.39	8	0.33	43.4	92	0.17	26.6
Adhesiveness (mJ)	0.01	12.43	8	0.30	39.6	92	0.33	26.6
Cohesiveness	0.01	1.05	8	0.33	24.0	92	0.33	26.6
Springiness (mm)	0	19.20	8	0.33	35.4	92	0.33	26.6

**Table 3**  
Comparison of predicted and measured responses.

Run	Response	Predicted value	Measured value	Accuracy
1	Hardness (N)	0.91	0.90	99%
	Adhesiveness (mJ)	1.4	2.1	50%
	Cohesiveness	0.33	0.27	82%
	Springiness (mm)	5.08	5.57	90%
2	Hardness (N)	5.391	4.705	87%

$$S = 29.6 + 0.392i + 34h - 2.13s + 0.0410s^2 \quad (4)$$

### 3.6. Effect of combined printing parameters on textural responses

The limitation of OFAT approach was evident as it overlooked interaction effects among parameters. An interaction effect is the simultaneous effect of two or more independent parameters on the output response, where their combined effect is significantly greater or smaller than the sum of the parts. The empirical model of hardness revealed interactions (1) between infill percentage (*i*) and layer height (*h*), and (2) between layer height (*h*) and print speed (*s*). The presence of interactions (i.e. (*i*)(*h*) and (*h*)(*s*)) in the model were statistically significant, as indicated by the *P*-value (0.05) in the ANOVA for hardness. Additionally, the curvature in the surface plots (Fig. 4) visually demonstrated the interaction effects between these variables, reinforcing the need for a comprehensive approach such as RSM.

Fig. 4A suggests that the joint effect of infill percentage (*i*) and layer height (*h*) on hardness (*H*) was observed at a constant printing speed (*s* = 35 mm/s). The maximum point of hardness (4.02 N) was obtained at the maximum and minimum values of infill percentage and layer height of 92% and 0.17 mm respectively. However, the minimum hardness point (0.08 N) occurred at the minimum value of infill percentage of 8%, and a layer height of 0.27 mm. This observation can be explained because the higher infill percentage resulted in the larger amount of material deposited within the internal structure in each layer. These printing parameters also led to a densely packed interior with less space between material layers, resulting in increased hardness. Additionally, the reduced layer height suggested that the increased number of layers were printed to fill the fixed height (15 mm), resulting in depositing an increased amount of materials per volume and further increasing hardness.

Fig. 4C shows the combined effect of layer height (*h*) and print speed (*s*) on hardness (*H*) at a constant infill percentage (*i* = 50%). According to the plot, the hardness decreased as print speed increased for low layer height (*h* = 0.17 mm). However, increasing print speed did not result in decreasing hardness for high layer height (*h* = 0.33 mm). This observation can be explained by the fact that increasing print speeds reduced the material deposited per unit length at a low layer height, resulting in decreased hardness. On the other hand, printing at a high layer height reduced the number of layers to reach a fixed height (15 mm). The printed layers were less compressed than those printed at a lower layer height. Therefore, increasing print speeds may have aided the layers to stack compactly, minimizing the formation of voids and porosity, and hence resulting in increased hardness. These hypotheses can be verified with further investigation.

### 3.7. Multi-response optimization and validation of models

The use of the multi-response optimization framework within the statistical software (Minitab) allows for the identification of the optimal combination of independent variables that optimize each textural response. Furthermore, this framework predicted the corresponding settings for an identified combination of independent variables (Table 2). For example, the predicted minimum and maximum hardness were 0.66 N and 5.39 N, respectively. The required parameters to achieve the minimum and maximum hardness were (*i* = 8%, *h* = 0.33 mm, *s* = 43.4 mm/s) and (*i* = 92%, *h* = 0.17 mm, *s* = 26.6 mm/s), respectively.

The accuracy of the developed models was tested and validated by performing multi-response optimizations with the cricket ink. In this work, accuracy was calculated using the following:

$$\text{Accuracy (\%)} = \left( 1 - \frac{|\text{Predicted value} - \text{Measured value}|}{\text{Predicted value}} \right) \times 100$$

The first run was to replicate the texture of other food and the second run was to achieve the maximum hardness. Mashed potato

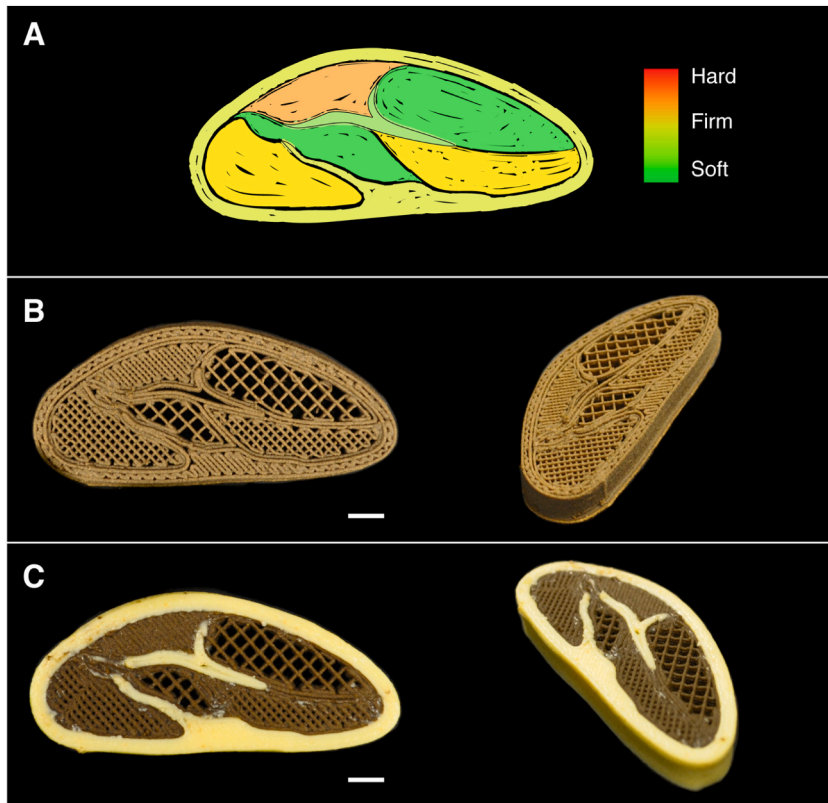


**Fig. 5.** DIW 3D-printed cricket steak with multi-infills. **A)** Illustration of a steak with different hardness in different areas. **B)** 3D printed steak containing cricket inks. 25%, 50% and 75% infill were used to produce soft, firm and hard texture respectively. **C)** 3D-printed multi-materials steak with cricket inks as alternative protein and milk as fats substitute. (All scale bars: 5 mm).

was selected as an example because the measured textural properties were within the achievable range of our inks (Table 2). The use of mashed potato as an example in our validation test was important because it allowed for a comparison between the texture of the 3D-printed food and the conventional food with similar textural properties.

Based on the measured textural properties of the mashed potato, we intended to predict adequate 3D printing parameters to replicate the same properties. Multiple combinations of the 3D printing parameters ( $i$ ,  $h$ ,  $s$ ) were suggested to fit the textural properties of the mashed potato. A set of the 3D printing parameters ( $i = 25\%$ ,  $h = 0.22$  mm, and  $s = 27.2$  mm/s) was selected to replicate the measured texture. With these parameters, the accuracy of the models for hardness, adhesiveness, cohesiveness, and springiness was 99%, 50%, 82%, and 87%, respectively (Table 3). These values suggested that simultaneously replicating all textural properties may be challenging. Based on equations (1)–(4), four textural properties ( $H$ ,  $C$ ,  $A$ ,  $S$ ) were predicted with three 3D printing parameters ( $i$ ,  $h$ ,  $s$ ). As such, these four equations do not have simultaneous solutions. The particular selection of the 3D printing parameters (that were suggested by the statistical software) was less effective in predicting the adhesiveness of the printed food than the other textural properties.

Despite the challenges of fitting all four textural properties simultaneously, the developed model was successfully used to replicate the value for a selected (single) textural property. For example, the model suggested that the highest hardness was obtained with the 3D printing parameters of  $i = 92\%$ ,  $h = 0.17$  mm,  $s = 26.6$  mm/s. The texture profile analysis suggested an accuracy of 87% for the hardness of the printed model. We note that the minimum and maximum limits of textural properties were determined for the formulated cricket ink (i.e., 40% w/w cricket powder and 0.4% w/w xanthan gum). These limits would vary with the concentrations of ingredients, or pre/post-treatments of the ink (such as steaming, frying, and baking). Overall, these results demonstrated the applicability of RSM to predict and control the texture of 3D-printed foods.

### 3.8. Varying textures with multiple materials

Finally, the combination of DIW printing with RSM was demonstrated to enable fabricating foods with varying textures at different locations. The variation of the texture can be readily achieved by employing multiple inks with different textures. However, our approach has enabled fabricating such foods only using the print conditions and the toolpath. To illustrate this capability, a model with the shape of a steak with varying infill percentages across the areas was created to create different textures (Fig. 5A and B). For example, using three different infill levels (e.g., 25%, 50%, and 75%) allowed producing the varying textures across the printed food

using a single material. In addition, multi-material food printing was readily performed by DIW printing to imitate real foods. As a demonstration, milk ink was used to illustrate the presence of fats in a steak model (Fig. 5C). This demonstration highlighted the potential to create 3D food products with multiple food materials with different textures.

#### 4. Conclusions

This research work investigated the use of response surface methodology (RSM) in 3D food printing to predict and control the texture of 3D-printed food products. Using CCD in RSM, we constructed empirical models for textural properties, including hardness ( $H$ ), adhesiveness ( $A$ ), cohesiveness ( $C$ ), and springiness ( $S$ ) while varying three parameters relevant to the control over the motion of the nozzle: (1) infill percentage ( $i$ ), (2) layer height ( $h$ ), and (3) print speed ( $s$ ). To achieve the desired textural properties, we used a response optimization framework to predict the values of 3D printing parameters. Our validation also affirmed the accuracy of our surface models and approach, which allowed predicting the texture of 3D-printed food. Finally, we demonstrated that DIW printing combined with RSM allowed for the fabrication of food with varying textures at different sections. We believe the current demonstration paves an avenue to customize the texture of food with 3D printing. The principles and methods discussed in this work should apply to other edible inks for DIW 3D printing, which should find potential applications in the healthcare and food industry.

#### CRedit authorship contribution statement

**Cheng Pau Lee:** Writing – review & editing, Writing – original draft, Visualization, Validation, Software, Methodology, Investigation, Formal analysis, Data curation, Conceptualization. **Michinao Hashimoto:** Writing – review & editing, Supervision, Resources, Project administration, Funding acquisition.

#### Declaration of competing interest

The authors declare that they have no known competing financial interests or personal relationships that could have appeared to influence the work reported in this paper.

#### Acknowledgements

C.P.L. acknowledged the financial support from the President's Graduate Fellowship awarded by Ministry of Education (MOE), Singapore. C.P.L. and M.H. thank International Design Centre (IDC) at SUTD for the project support (IDG11700103 - Digital Fabrication of Edible Materials) and SUTD Growth Plan (SGP) in Healthcare Research (SGPHCRS1907 - Thrust 3-3: 3D Food Printing), SUTD Kickstarter Initiative Grants (SKI 2021\_02\_09).

#### Appendix A. Supplementary data

Supplementary data to this article can be found online at <https://doi.org/10.1016/j.heliyon.2024.e27658>.

#### References

- [1] C.P. Lee, M. Takahashi, S. Arai, C.-L.K. Lee, M. Hashimoto, 3D printing of Okara ink: the effect of particle size on the printability, *ACS Food Sci. Technol.* 1 (11) (2021) 2030–2191.
- [2] S. Mantihal, S. Prakash, B. Bhandari, Texture-modified 3D printed dark chocolate: sensory evaluation and consumer perception study, *J. Texture Stud.* 50 (5) (2019) 386–399.
- [3] Z. Liu, B. Bhandari, S. Prakash, M. Zhang, Creation of internal structure of mashed potato construct by 3D printing and its textural properties, *Food Res. Int.* 111 (2018) 534–543.
- [4] X. Wang, Q. Ao, X. Tian, J. Fan, H. Tong, W. Hou, S. Bai, Gelatin-based hydrogels for organ 3D bioprinting, *Polymers* 9 (9) (2017) 401.
- [5] N. Noor, A. Shapira, R. Edri, I. Gal, L. Wertheim, T. Dvir, 3D printing of personalized thick and perfusable cardiac patches and hearts, *Adv. Sci.* 6 (11) (2019) 1900344.
- [6] K. Yamagishi, W. Zhou, T. Ching, S.Y. Huang, M. Hashimoto, Ultra-deformable and tissue-adhesive liquid metal antennas with high wireless powering efficiency, *Adv. Mater.* 33 (26) (2021) 2008062.
- [7] A.A. Shapiro, J.P. Borgonia, Q.N. Chen, R.P. Dillon, B. McEnerney, R. Polit-Casillas, L. Soloway, Additive manufacturing for aerospace flight applications, *J. Spacecraft Rockets* 53 (5) (2016) 952–959.
- [8] Q. Zhu, Z. Liu, J. Yan, Machine learning for metal additive manufacturing: predicting temperature and melt pool fluid dynamics using physics-informed neural networks, *Comput. Mech.* 67 (2) (2021) 619–635.
- [9] N. Nadammal, M. Rajput, S.K. Gupta, E. Ivanov, A.S. Reddy, S. Suwas, K. Chatterjee, Laser powder bed Fusion additive manufacturing of a low-modulus Ti-35Nb-7Zr-5Ta alloy for orthopedic applications, *ACS Omega* 7 (10) (2022) 8506–8517.
- [10] T. Ching, Y. Li, R. Karyappa, A. Ohno, Y.-C. Toh, M. Hashimoto, Fabrication of integrated microfluidic devices by direct ink writing (DIW) 3D printing, *Sensor. Actuator. B Chem.* 297 (2019) 126609.
- [11] W.H. Goh, M. Hashimoto, Fabrication of 3D microfluidic channels and in-channel features using 3D printed, water-soluble sacrificial mold, *Macromol. Mater. Eng.* 303 (3) (2018) 1700484.
- [12] X. Xie, S. Maharjan, C. Kelly, T. Liu, R.J. Lang, R. Alperin, S. Sebastian, D. Bonilla, S. Gandolfo, Y. Boukataya, S.M. Siadat, Y.S. Zhang, C. Livermore, Customizable microfluidic origami liver-on-a-chip (oLOC), *Adv. Mater. Technol.* (2021) 2100677.

- [13] Z. Zhao, Q. Li, L. Chen, Y. Zhao, J. Gong, Z. Li, J. Zhang, A thread/fabric-based band as a flexible and wearable microfluidic device for sweat sensing and monitoring, *Lab Chip* 21 (5) (2021) 916–932.
- [14] S.R. Shin, R. Farzad, A. Tamayol, V. Manoharan, P. Mostafalu, Y.S. Zhang, M. Akbari, S.M. Jung, D. Kim, M. Comotto, N. Annabi, F.E. Al-Hazmi, M.R. Dokmeci, A. Khademhosseini, A bioactive carbon nanotube-based ink for printing 2D and 3D flexible electronics, *Adv. Mater.* 28 (17) (2016) 3280–3289.
- [15] H. Zhu, X. Hu, B. Liu, Z. Chen, S. Qu, 3D printing of conductive hydrogel-elastomer hybrids for stretchable electronics, *ACS Appl. Mater. Interfaces* 13 (49) (2021) 59243–59251.
- [16] R. Karyappa, M. Hashimoto, Chocolate-based ink three-dimensional printing (Ci3DP), *Sci. Rep.* 9 (1) (2019) 14178.
- [17] S.M. Kim, J.H. Woo, H.W. Kim, H.J. Park, Formulation and evaluation of cold-extruded chocolate ganache for three-dimensional food printing, *J. Food Eng.* 314 (2022) 110785.
- [18] S. Zhu, I.V. Ruiz de Azua, S. Feijen, A.J. van der Goot, M. Schutyser, M. Stieger, How macroscopic structure of 3D printed protein bars filled with chocolate influences instrumental and sensory texture, *LWT* 151 (2021) 112155.
- [19] C.P. Lee, R. Karyappa, M. Hashimoto, 3D printing of milk-based product, *RSC Adv.* 10 (50) (2020) 29821–29828.
- [20] F. Yang, Y. Cui, Y. Guo, W. Yang, X. Liu, X. Liu, Internal structure and textural properties of a milk protein composite gel construct produced by three-dimensional printing, *J. Food Sci.* 86 (5) (2021) 1917–1927.
- [21] J.J.Y. Tan, C.P. Lee, M. Hashimoto, Preheating of gelatin improves its printability with transglutaminase in direct ink writing 3D printing, *Int. J. Bioprint.* 6 (4) (2020) 296.
- [22] N. Carvajal-Mena, G. Tabilo-Munizaga, M. Pérez-Won, R. Lemus-Mondaca, Valorization of salmon industry by-products: evaluation of salmon skin gelatin as a biomaterial suitable for 3D food printing, *LWT* 155 (2022) 112931.
- [23] A. Pant, A.Y. Lee, R. Karyappa, C.P. Lee, J. An, M. Hashimoto, U.X. Tan, G. Wong, C.K. Chua, Y. Zhang, 3D food printing of fresh vegetables using food hydrocolloids for dysphagic patients, *Food Hydrocolloids* 114 (2021) 106546.
- [24] H.W. Kim, J.H. Lee, S.M. Park, M.H. Lee, I.W. Lee, H.S. Doh, H.J. Park, Effect of hydrocolloids on rheological properties and printability of vegetable inks for 3D food printing, *J. Food Sci.* 83 (12) (2018) 2923–2932.
- [25] Y. Chen, M. Zhang, P. Phuhongsung, 3D printing of protein-based composite fruit and vegetable gel system, *LWT* 141 (2021) 110978.
- [26] A. Derossi, R. Caporizzi, D. Azzollini, C. Severini, Application of 3D printing for customized food. A case on the development of a fruit-based snack for children, *J. Food Eng.* 220 (2018) 65–75.
- [27] J. Sun, Z. Peng, L. Yan, J. Fuh, G.S. Hong, 3D food printing—an innovative way of mass customization in food fabrication, *Int. J. Bioprint.* 1 (1) (2015) 1.
- [28] I. Dankar, A. Haddarah, F.E.L. Omar, F. Sepulcre, M. Pujolà, 3D printing technology: the new era for food customization and elaboration, *Trends Food Sci. Technol.* 75 (2018) 231–242.
- [29] C.P. Lee, J.Y. Hoo, M. Hashimoto, Effect of oil content on the printability of coconut cream, *Int. J. Bioprint.* 7 (2) (2021) 354.
- [30] M.-s. Huang, M. Zhang, B. Bhandari, Assessing the 3D printing precision and texture properties of Brown rice induced by infill levels and printing variables, *Food Bioprocess Technol.* 12 (7) (2019) 1185–1196.
- [31] E.K. Hadde, J. Chen, Texture and texture assessment of thickened fluids and texture-modified food for dysphagia management, *J. Texture Stud.* 52 (1) (2021) 4–15.
- [32] A. Souto, J. Zhang, A.M. Aragon, K.P. Velikov, C. Coulais, Edible mechanical metamaterials with designed fracture for mouthfeel control, *Soft Matter* 18 (15) (2022) 2910–2919.
- [33] C. Feng, M. Zhang, B. Bhandari, Y. Ye, Use of potato processing by-product: effects on the 3D printing characteristics of the yam and the texture of air-fried yam snacks, *LWT* 125 (2020) 109265.
- [34] D.C. Montgomery, in: *Introduction to Statistical Quality Control*, sixth ed., Wiley, Hoboken, NJ, 2009.
- [35] M.T. Espino, B.J. Tuazon, A.H. Espera, C.J.C. Nocheseda, R.S. Manalang, J.R.C. Dizon, R.C. Advincula, Statistical methods for design and testing of 3D-printed polymers, *MRS Commun* 13 (2) (2023) 193–211.
- [36] Y.K. M, Harsh Vardhan Rai, Ashay Pare, Process parameter optimization for tensile strength of 3D printed parts using response surface methodology, *IOP Conf. Ser. Mater. Sci. Eng.* 377 (2018) 012027.
- [37] S. Dey, N. Hettiarachchy, A.A. Bisly, K. Luthra, G.G. Atungulu, A. Ubeyitogullari, L.A. Mozzoni, Physical and textural properties of functional edible protein films from soybean using an innovative 3D printing technology, *J. Food Sci.* 87 (11) (2022) 4808–4819.
- [38] G. Yang, Y. Tao, P. Wang, X. Xu, X. Zhu, Optimizing 3D printing of chicken meat by response surface methodology and genetic algorithm: feasibility study of 3D printed chicken product, *LWT* 154 (2022) 112693.
- [39] L. Liu, X. Yang, B. Bhandari, Y. Meng, S. Prakash, Optimization of the formulation and properties of 3D-printed complex egg white protein objects, *Foods* 9 (2) (2020) 164.
- [40] Y.-J. Lin, P. Punpongsonan, X. Wen, D. Iwai, K. Sato, M. Obrist, S. Mueller, FoodFab: creating food perception illusions using food 3D printing, in: *Proceedings of the 2020 CHI Conference on Human Factors in Computing Systems*, 2020, pp. 1–13.
- [41] A.S. Szczesniak, Texture is a sensory property, *Food Qual. Prefer.* 13 (4) (2002) 215–225.
- [42] C. da Rosa Machado, R.C.S. Thys, Cricket powder (*Gryllus assimilis*) as a new alternative protein source for gluten-free breads, *Innov. Food Sci. Emerg. Technol.* 56 (2019) 102180.
- [43] Thailand Unique, 2022. <https://www.thailandunique.com/insect-bug-flour-powder/kilogram-cricket-powder>. (Accessed 28 April 2022).
- [44] J. Werthmann, A. Jansen, R. Havermans, C. Nederkoorn, S. Kremers, A. Roefs, Bits and pieces. Food texture influences food acceptance in young children, *Appetite* 84 (2015) 181–187.
- [45] N. Pematilleke, M. Kaur, C.T. Rai Wai, B. Adhikari, P.J. Torley, Effect of the addition of hydrocolloids on beef texture: targeted to the needs of people with dysphagia, *Food Hydrocolloids* 113 (2021) 106413.
- [46] W.Y. Jeon, J.Y. Yu, H.W. Kim, H.J. Park, Production of customized food through the insertion of a formulated nanoemulsion using coaxial 3D food printing, *J. Food Eng.* 311 (2021) 110689.
- [47] Y. Zhao, G. Yang, L. Zhu, Y. Ding, X. Guan, X. Wu, Z. Yang, Effects of rheological properties and printing speed on molding accuracy of 3D printing basalt fiber cementitious materials, *J. Mater. Res. Technol.* 21 (2022) 3462–3475.